Modeling of Clogging and Erosion of Nozzle Refractories in Steel Casting

O. Araromi, B. G. Thomas, E. Conzemius

Department of Mechanical Science and Engineering
University of Illinois at Urbana-Champaign,
1206 West Green Street, Urbana, IL 61801, USA

Abstract

The walls of nozzle refractories in steelmaking processes can clog or erode, depending on their composition relative to the inclusions in the steel. Both problems can lead to severe inclusion problems in the cast product. Fundamental computational models are developed to study the complex coupled phenomena which govern this process: the turbulent flow of molten steel through the nozzle, contacting of solid inclusions in the steel with the nozzle wall, heat transfer in the wall and steel, species diffusion through the nozzle wall, and the thermodynamics of the chemical reactions that form solid precipitates, or change the composition of the inclusions to liquefy them, allowing them to erode from the walls. A case study is simulated in this work for clogging prevention in CaO-bearing nozzles by partial liquefying of the Al_2O_3 inclusions. The model is validated with measurements of erosion rate and composition variations in the wall. Such models offer potential for new quantitative insights into these phenomena.

Keywords: doloma, alumina, nozzle, clogging, erosion, inclusions, reactions, diffusion, models

Background

Nozzle clogging is a serious productivity and quality problem the commonly plagues the steel industry. Clogging is caused by buildup of non-metallic inclusions on the nozzle walls. Inclusions come from upstream deoxidation products, reoxidation, and reactions with the nozzle refractory material [1]. Clogging restricts the flow between the tundish and continuous casting mold, shortening the time between costly nozzle changes. Clogging lowers product quality by causing: 1) nonuniform flow variations leading to mold level variations; and 2) many large inclusions, level variations, and slag composition problems when clogs suddenly dislodge and enter the mold.

Alumina inclusions readily sinter and attach to the walls of alumina-refractory nozzles. As clogging progresses, steel trapped between particles can solidify and support the fragile structure, allowing clogging to proceed. Using doloma as the nozzle refractory material can disrupt clogging by preventing alumina inclusions from sticking to the nozzle walls [2, 3]. As illustrated in Fig. 1, this is accomplished by the diffusion of some CaO from the nozzle into each Al_2O_3 inclusion. This changes the inclusion composition, causing them to partially liquefy, and become more spherical, so they are easily washed away from the interface by the turbulent flow. While preventing alumina clogs and extending nozzle life, this mechanism slowly erodes the nozzle wall. Figure 2 shows typical clogging of an alumina nozzle [1], and erosion of a doloma nozzle [4].

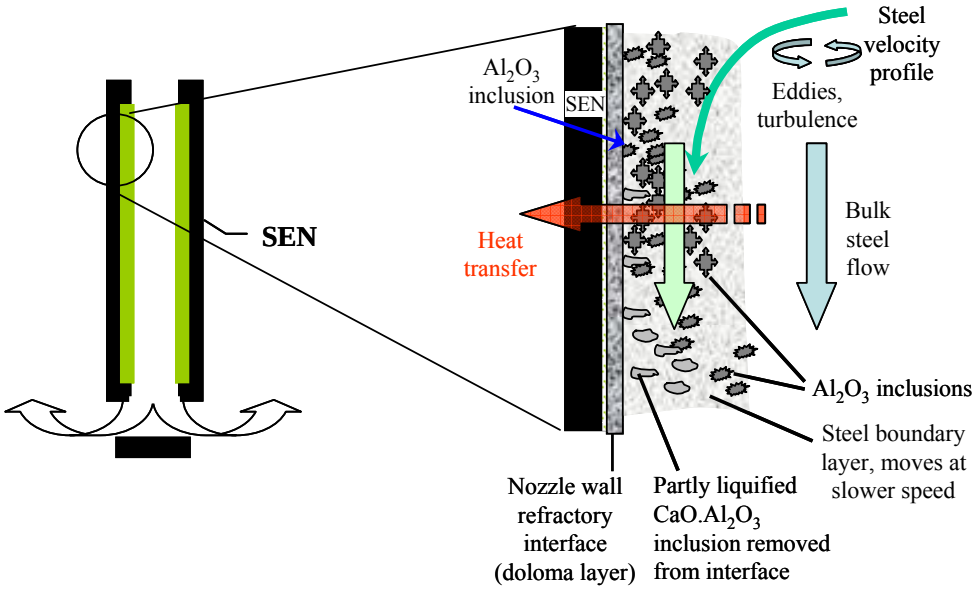

Fig. 1 – Phenomena in nozzle clogging and prevention by CaO refractory wall erosion

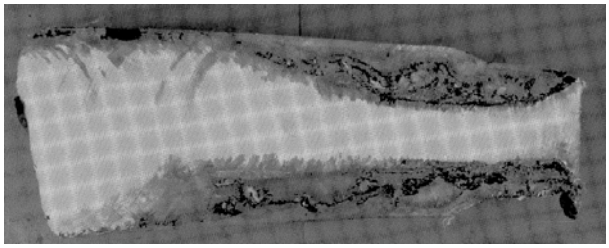

a) Alumina-graphite nozzle after freeze-off showing alumina clogging mixed with steel

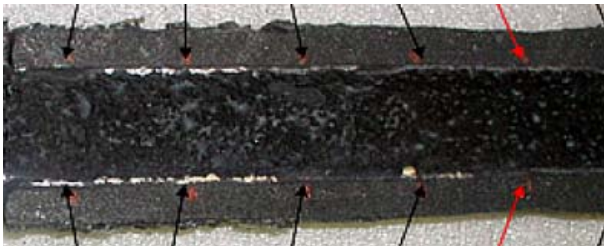

b) Doloma (CaO-MgO) nozzle showing some wall erosion, but no clogging

Fig. 2 – Typical continuous-casting submerged entry nozzles after several hours of operation

The attachment of inclusions to the nozzle wall depends on many complex phenomena, First is the turbulent fluid flow pattern and trajectories inside the nozzle that bring inclusions to contact the wall and / or wash them away. Many additional complex coupled phenomena affect attachment at the particle-refractory interface, including heat conduction, multi-component, multi-phase thermodynamics, ion-diffusion (through the bulk, solid-phase, liquid-phase, and grain boundaries), phase transformations, chemical reactions (such as graphite oxidation, spinel formation), and the shape of the interface and particle.

As an initial attempt to quantify these phenomena, this paper presents a one-dimensional finite-element model of alumina inclusions contacting a doloma nozzle wall. The model is applied to predict the dissolution and sweeping away of alumina inclusions, composition evolution and liquefaction of the nozzle wall, wall erosion rate, and the removal rate and composition of released inclusions.

Model Description

The nozzle erosion / clogging mechanism at the microscopic scale is considered to evolve in 3 stages, illustrated in Fig. 3:

1) Each inclusion that touches wall surface causes diffusion, partially liquefies, and is then carried away with the bulk flow of molten steel, and also causing some small erosion of the nozzle wall. Although its surface composition changes, the remaining wall is completely solid.
2) The alumina accumulated at the nozzle from many inclusions causes gradual liquefying of the surface layer of the nozzle wall, entrainment of inclusions that touch, and formation of liquid/inclusion matrix layers in the wall.
3) Inclusions build up on the nozzle surface faster than CaO can be supplied, so the nozzle wall can no longer liquefy all the inclusions present at the interface. Thus, clogging can proceed. This stage is likely if the inclusion build-up is too fast, such as due to a local reoxidation problem. The force of the flowing steel can wash away large chunks of the fragile liquefied layer, leading to wide variations in wall thickness.

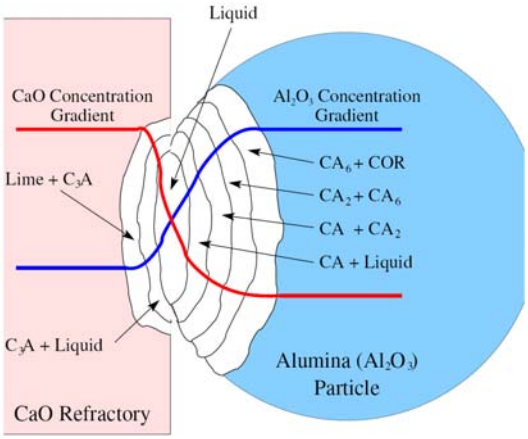

Fig. 3 a) – Stage 1 model [5]: Diffusion exchange of CaO and Al_2O_3 liquefies the surface of an Al_2O_3, inclusion, allowing it to be removed by the flowing steel.

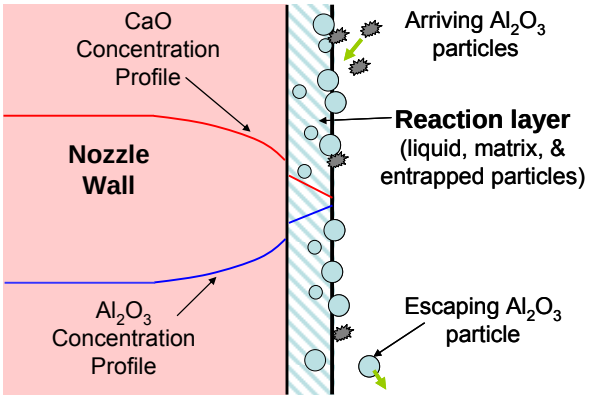

Fig. 3 b) – Stage 2 model: Diffusion builds up partly-liquefied reaction layer at nozzle surface.

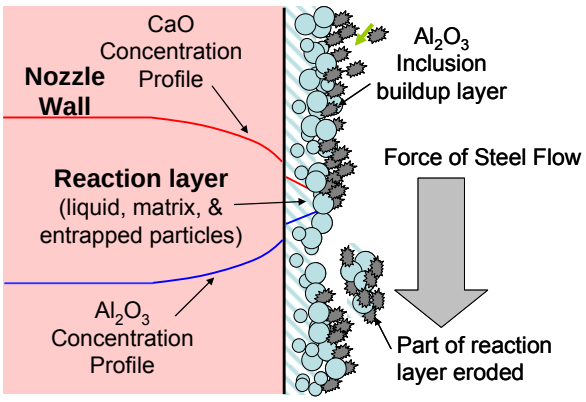

Fig. 3 c) – Stage 3 model: Excessive inclusion buildup allows clogging and wall erosion.

A computational model has been developed of each stage [6, 7]. The model solves the transient one-dimensional diffusion equation, using the finite-element method. To accommodate different activity coefficients in different phases, and the corresponding jumps in concentration at the interfaces, the equation is formulated in terms of activity:

$$\frac{\partial a_\alpha}{\partial t} = \frac{\partial}{\partial x}\left(D_\alpha \frac{\partial a_\alpha}{\partial x} \right) \tag{1}$$

where a_α is activity of phase α, D is diffusivity (m^2/s), x is distance through nozzle and inclusion (m), and t is time (s). Concentration C (weight percent) is found from the activity field by dividing by the activity coefficient. Assuming activity coefficients are unity, Eq. 1 simplifies to:

$$\frac{\partial C_\alpha}{\partial t} = \frac{\partial}{\partial x}\left(D_\alpha \frac{\partial C_\alpha}{\partial x} \right) \tag{2}$$

For the diffusion of ionic species that make up ceramic refractories, the model assumes that ions are always exchanged to maintain charge balance. Thus, diffusion is controlled by the slower diffusing species. This enables solving a single diffusion equation for Al_2O_3 concentration in the doloma (calcia-magnesia-alumina) refractory, as molar diffusion of CaO is assumed equal and opposite. Mass flow rate of Ca is 2/3 of (26.98 g/mol) / (40.08 g/mol) of the calculated Al diffusion mass flow rate (kg/s). Diffusion of the MgO is neglected, although its concentration changes due to the mass flows of the other components. Other components, such as graphite, are ignored. Inclusion particles are assumed to be composed entirely of alumina.

The model domain is generally a semi-infinite part of the surface region of the nozzle wall. For stage 1 the domain extends through the inclusion as well. The inclusion is assumed to be spherical, so the cross-sectional area of successive sections changes with distance into the inclusion. The contact area at the wall is an input parameter.

The domain starts with a solid wall region with no alumina (left), contacting a region of solid inclusion(s) of alumina (right). As the two regions interact, a liquid region forms between the two solid regions. In Stage 1, the liquid that forms is removed with the inclusion. Inclusions are continuously replaced, and are assumed to vary contacting points so that the concentration profiles remain one dimensional. In Stage 2, the alumina is assumed to accumulate in the nozzle surface, enabling up a thick liquid layer to build up with time.

Equation (2) is discretized in space using the standard finite-element method,

$$\sum [C]\{\dot{C}_\alpha\} + \sum [D]\{C_\alpha\} = \sum \{F\} \tag{3}$$

where $\{\dot{C}_\alpha\}$ is discretized in time using the explicit central-difference method. $\{F\}$ is the force matrix, which contains only terms from the previous time step, as there are no mass sources, and the boundary conditions of the semi-infinite domain are mathematically insulated. Standard two-node linear elements with a lumped capacitance matrix are used.

$$[D] = \frac{A_j D_\alpha^j}{L_j}\begin{bmatrix} 1 & -1 \\ -1 & 1 \end{bmatrix}; \quad [C_j] = \begin{bmatrix} 0.5 & 0 \\ 0 & 0.5 \end{bmatrix} A_j L_j \tag{4}$$

where the element diffusivity is calculated from a geometric average of the diffusivities at its two nodes. Diffusion coefficients are composition-dependent and vary greatly between the three layers. The effect of temperature gradients is ignored, owing to the small domain thickness.

Model Validation with Analytical Solution

The model was first validated by comparison with an analytical solution for 1-D diffusion through a 3-layer wall, developed by Maske [5]. The analytical model solves the classic 1-D transient diffusion equation in each layer, using the following similarity solution, assuming a different constant diffusion coefficient in each layer.

$$C_\alpha = C_{\alpha 0} - \frac{(C_{\alpha 0} - C_{\alpha\beta})}{1 + erf\left(\varsigma_{\alpha\beta}\sqrt{D_\beta / D_\alpha}\right)}\left(1 + erf\left(\frac{x}{\sqrt{4D_\alpha t}}\right)\right) \tag{5}$$

$$C_\beta = C_{\alpha\beta} - \frac{(C_{\alpha\beta} - C_{\beta\gamma})}{erf\,\varsigma_{\beta\gamma} - erf\,\varsigma_{\alpha\beta}}\left(erf\left(\frac{x}{\sqrt{4D_\beta t}}\right) - erf\,\varsigma_{\alpha\beta}\right) \tag{6}$$

where C is concentration, β is the middle phase layer, αβ and αγ refer to the interfaces between the 3 layers, and the two ζ parameters are solved by performing a species mass balance at those interfaces [5]. Distance x is measured from zero at the original interface between the α (left) and γ (right) layers, which start at time t=0 with different constant initial concentrations $C_{\alpha 0}$ = 1 and $C_{\gamma 0}$ = 0. The interfaces advance in opposite directions from x=0 in proportion to the square root of time, as the middle layer grows:

$$x_{\alpha\beta} = 2\varsigma_{\alpha\beta}\sqrt{4D_\beta t} \quad x_{\beta\gamma} = 2\varsigma_{\beta\gamma}\sqrt{4D_\beta t} \tag{7}$$

For an example to simulate a liquid layer forming between two solid layers, the middle liquid layer was given a "high" diffusion coefficient, D_β = 2.0× 10^{-2} mm^2/s, and the infinite solid layers on its left and right were each given the "low" value of D_α = 7.0× 10^{-3} mm^2/s. The interfaces where the diffusion coefficients change were defined by $C_{\alpha\beta}$=0.9 and $C_{\beta\gamma}$=0.1. For simplicity, activity coefficients were assumed unity, so concentration and activity are equal, and no discontinuities arise at the phase interfaces. Using a fine mesh of 250 nodes, the finite-element model almost exactly coincides with the analytical solution, as the snapshot in Fig. 4 shows at 10^{-6}s. By this time, the interface has grown to ~0.27 μm in each direction.

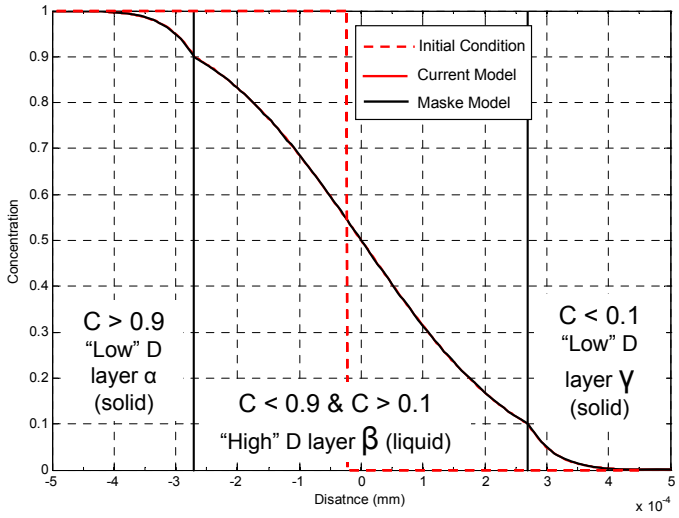

Fig. 4 Snapshot comparing analytical and computational model concentration profiles in wall

Diffusivity Model

Realistic coefficients for alumina diffusion were chosen, based on phase fractions found using the Alumina-Calcia-Magnesia ternary phase diagram. Specifically, $D_\alpha=10^{-8}$ m^2/s in the calcia-rich solid wall, $D_\beta=10^{-5}$ m^2/s in the liquid reaction zone and $D_\gamma=10^{-11}$ m^2/s in the alumina-rich particle layer. The effective diffusivity of liquid D_β was assigned in phase regions containing over 50% liquid, and solid was defined in regions containing less than 5% liquid. An example section through the phase diagram at 1600 °C is shown in Fig. 5. The large white parts of the phase diagram are transition or mixed (M) phase regions, where diffusion coefficient was computed using a geometric average as follows:

$$D = D_\alpha^{\left(\frac{C_{M\beta}-C}{C_{M\beta}-C_{\alpha M}}\right)} \times D_\beta^{\left(\frac{C-C_{\alpha M}}{C_{M\beta}-C_{\alpha M}}\right)}; \quad D = D_\beta^{\left(\frac{C-C_{\beta M}}{C_{M\gamma}-C_{\beta M}}\right)} \times D_\gamma^{\left(\frac{C_{M\gamma}-C}{C_{M\gamma}-C_{\beta M}}\right)} \qquad (8)$$

With low MgO content, the transition region on the right side of Fig. 5 is never reached. Figure 6 shows the effective diffusivity as a function of composition, for a 10% MgO refractory. It also represents the diffusivity profile across the Stage 1 model domain. Diffusivity increases greatly as liquid forms, as convection mixing can occur along the grain boundaries, which liquefy first. An exponential increase in diffusivity occurs as the boundaries link together into a continuous network. This is why the diffusion coefficients assumed in the liquid region here are so much larger than the in the solid. Further fundamental work is needed to better quantify these diffusion coefficients.

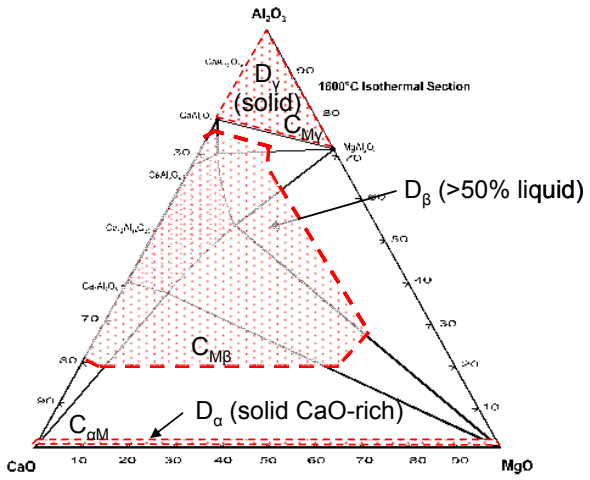

Fig. 5 – Al_2O_3 – CaO – MgO ternary phase diagram at 1600 °C, showing phase regions used to define diffusion coefficients

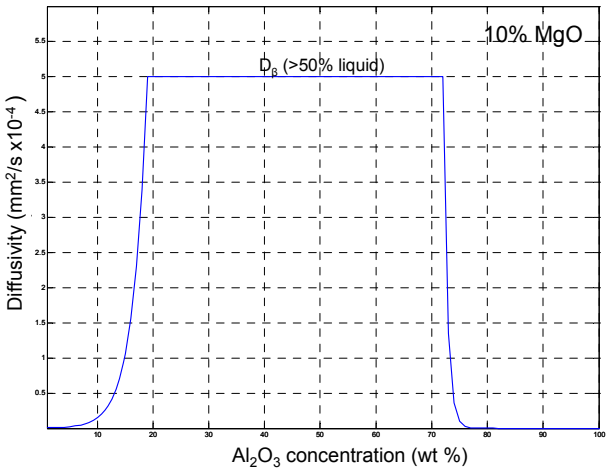

Fig. 6 – Diffusion coefficient profile across model domain

Typical Results

A computational model simulation was performed for alumina inclusions contacting a nozzle refractory initially composed initially of 90% CaO and 10% MgO. Pure spherical alumina inclusions with 100 μm diameter contacted the surface in a continuous series, with an

assumed contact area of 20 μm (4% of the maximum cross-sectional area). Constant temperature of 1600 °C was assumed throughout.

Stage 1

An example of the composition profile in a typical particle from stage 1 is shown in Fig. 7 at 14.05s after start of casting. The profiles in both the particle and wall surface are established almost immediately and the interface (*x=0*) slowly migrates left, as the nozzle surface is eroded. The profile in Fig. 7 shows how alumina has diffused away and calcia has diffused into the particle. The particle contains very little CaO because only a small amount of diffusion is needed to liquefy the surface. The critical liquefied layer thickness depends on the force exerted by the flowing fluid and was assumed here to be 20 μm.

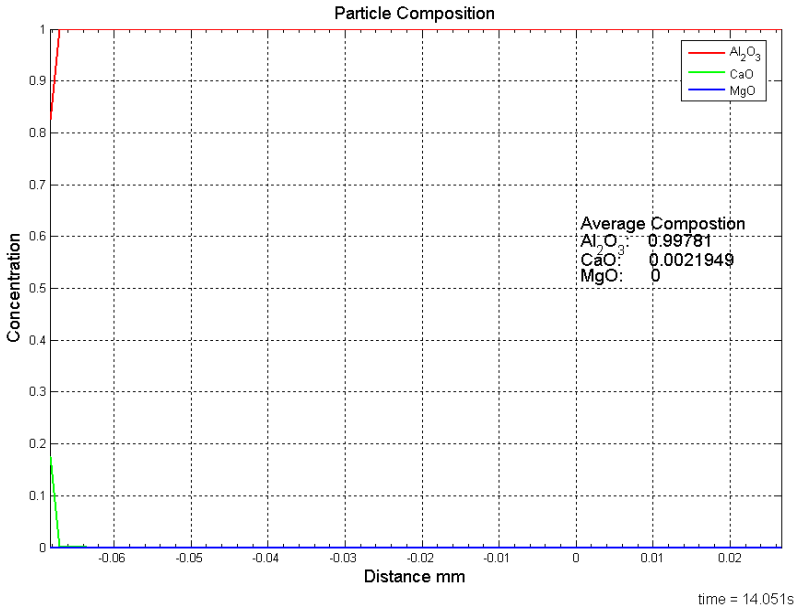

Fig. 7 – Stage 1 Composition profile in particle

Stage 2

A stage 2 simulation for the same conditions was performed, assuming 100% alumina fixed on the right boundary, to represent saturation with alumina inclusions at the surface. Erosion was neglected, so that the results can be interpreted as desired. The composition profile after 190 minutes (11,400s) is shown in Fig. 8.

The composition profiles show several expected features. As alumina diffuses into the nozzle surface from the inclusions, an alumina gradient extends into the nozzle. In addition, a reaction layer containing liquefied CaO-Al_2O_3 compounds is predicted to form and grow with time. The total thickness of this layer reaches 3.65mm. The liquefied portion of the layer is just slightly thinner (3.1mm). In reality, some of this layer could be eroded by the force of the molten steel flowing down through the nozzle. The model also predicts that liquefied inclusions could potentially increase the nozzle thickness (by 2.2mm in this case), if there is no erosion. Thus, the maximum total liquefied layer thickness is 5.3mm in ~3 hours.

The CaO profile naturally shows the expected decreasing gradient towards the interface, as it is depleted to the inclusions. A non-physical jump at the original interface occurs, due to lack of MgO diffusion into the new liquefied layer (x>0). The gradual increase in MgO concentration towards the surface is expected, as the CaO is depleted.

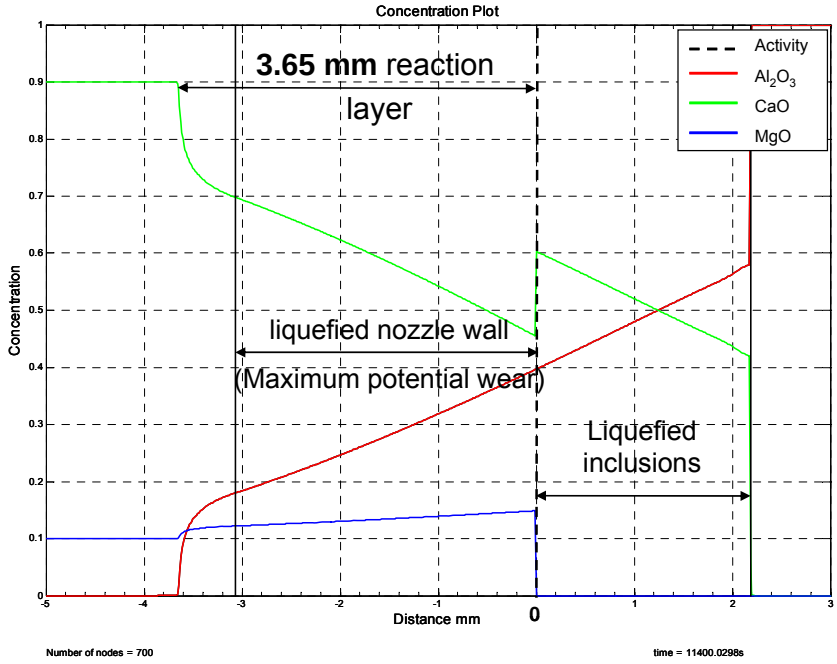

Fig. 8 Stage 2 Composition profile in nozzle wall near surface

Computations were then made based on these results to predict erosion rates [7]. Based on the 3.1mm thick eroded layer in 190 mins, 3360 kg/m^3 CaO density, CaO is removed at a rate of 8 x10^{-4} kg/m^{2}s. For a typical 1-m-long nozzle with 60-mm diameter, and a typical steel casting rate of 1.8 tonne/min, this corresponds to 5.2 ppm CaO in the steel product. If the nozzle was able to operate continuously in Stage 1, then much less CaO would enter the steel for the same clogging protection, owing to the smaller CaO content of individual particles compared with eroded pieces of the reaction layer. Based on the 2.2mm inclusion layer assumed to be removed, this calcia is able to liquefy over 4ppm of alumina. Further assuming about 10% of the inclusions contact the nozzle walls [1], this means that the nozzle should be able to continuously liquefy steel containing 40ppm of inclusions without allowing any clogging, at least for the first 3 hours. Assuming half of the total liquified layer is washed away, the corresponding nozzle wall erosion rate is on the order of ~1mm of wall thickness per hour.

Nozzle Measurements for Model Validation

The model was validated by comparing the model predictions with a case where measurements were conducted on a typical operating doloma nozzle [8]. A doloma-graphite submerged-entry nozzle (45%CaO, 35%MgO) was used successfully to cast forging steel for 191 minutes without clogging, and subsequently analyzed. Careful measurements of the nozzle wall showed that it was eroded 2~5mm near the SEN bottom but less than 1-mm near the SEN top, as shown in Fig. 9. The regions with highest wear near nozzle bottom showed thin (1~2mm)

reaction layers, while the low-wear regions near nozzle top showed reaction layers of 4~5mm in thickness. This is consistent with the model predictions of a total reaction layer thickness of ~5mm, with erosion removing portions of the reaction layer at different rates in different locations. Typical micrographs are shown in Fig. 9, and are arranged to illustrate these numbers.

Scanning electron microscope analysis of the reaction layer revealed elevated concentrations of Fe, Al and S, and depleted concentrations of Mg and Si. This provides evidence of a surface reaction layer containing infiltrated steel and alumina diffusion / capture that led to calcium aluminates / CaA_x (presumably liquid during casting), in addition to unreacted grains of magnesia from the original doloma. There is also evidence of CaS, presumably from reaction with S in the steel, and gas pores, presumably from graphite reactions. Beneath the reaction layer, the micrographs also reveal a 1-2.5 mm thick layer of carbon depletion before finally reaching the original unreacted doloma. Clearly, there are many phenomena yet to consider in the model.

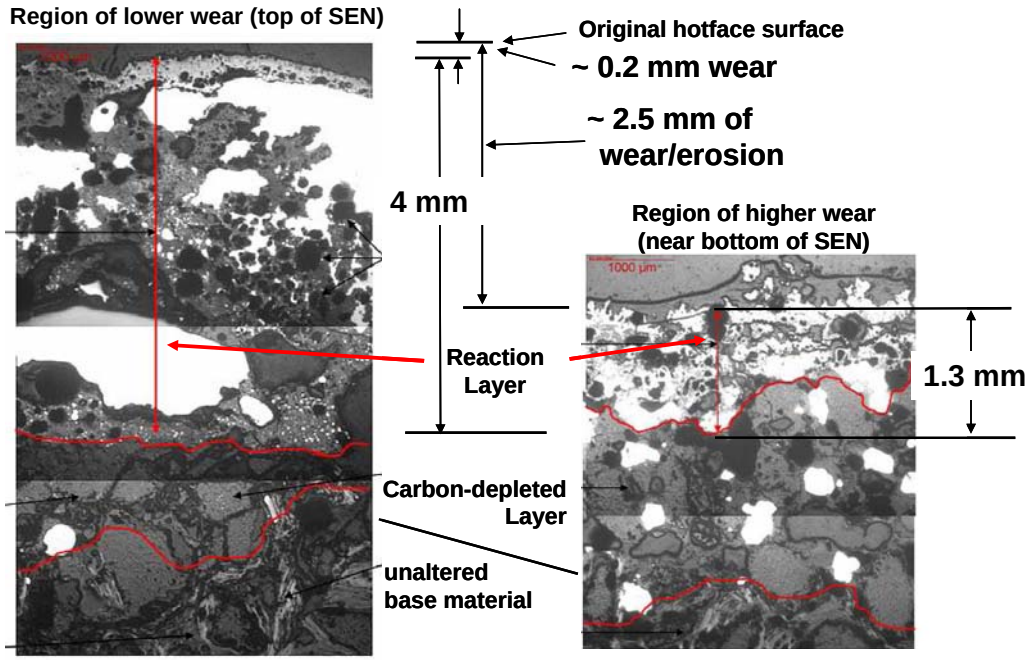

Fig. 9 - Microstructure near nozzle surface showing unaltered doloma refractory, carbon-depleted layer, and reaction layer, which is slightly eroded near SEN top (left) and greatly eroded near SEN bottom (right)

Conclusions

A detailed mechanistic 3-stage model has been developed to simulate diffusion, liquification, composition changes, and erosion of nozzle refractory walls. It is a macroscopic one-dimensional finite-element diffusion model, with different coefficients in each of three phase layers. The model has been validated with an analytical solution, and applied to simulate ~3 hours of service life of a typical doloma nozzle, where measurements were available. Finally, the model results can be interpreted to predict practical parameters such as erosion rate.

The doloma nozzles in the present study appear to have eroded at an average rate of ~1mm/hour and liquefied over 4ppm of alumina, which likely corresponds to clogging protection from ~40ppm total alumina inclusions in the flowing steel. The model predictions are roughly consistent with the measurements, considering the many crude assumptions. With much further work, this promising model could become a useful tool.

Acknowledgments

The authors wish to thank the Continuous Casting Consortium for support of this research, and Roy Maske for initial work on the project. Special thanks are extended to Rob Nunnington and Don Griffon for providing data and valuable discussions to help this work.

References

[1] K.G. Rackers and B.G. Thomas: "Clogging in Continuous Casting Nozzles," in *Steelmaking Conf. Proc.*, vol. 78, (Nashville, TN, April 2-5, 1995), Nashville, TN, 1995, pp. 723-734.
[2] G. T. Moulden and R. Sabol: "Development of Doloma Tundish Nozzles to Reduce Alumina Clogging," in *Steelmaking Conf. Proc.*, vol. 83, Pittsburgh, PA, 2000, pp. 161-166.
[3] Koji Ogata, Katsumi Morikawa, Arito Mizobe, Jiro Amano and Keisuke Asano: "Refractory Technology for Improvement of Steel Quality and Productivity," *Proc. AISTech Conference*, Charlotte, NC, May 9-11, 2005, 2005, vol. 1, pp. 175-184.
[4] D. Griffin and R. Nunnington: LWB Refractories, York, PA, private communication, 2007.
[5] Roy Maske, Preliminary Calculations for the Diffusion Couple of Calcia (CaO) and Alumina (Al203) Related to Nozzle Clogging in the Continuous Casting of Steel, ME550 Report, 2005, University of Illinois at Urbana-Champaign, May 12, 2005.
[6] Oluwaseun A. Araromi, Independent project on the prediction of Calcia (CaO) Alumina (Al_2O_3) - Attachment and removal in nozzles for the continuous casting of Steel to minimize clogging, 2005, ME497 Report, University of Illinois, Urbana, Illinois, May 10, 2005.
[7] Oluwaseun A. Araromi, Modeling of Clogging / Erosion of Nozzle Refractories, 2007, Continuous Casting Consortium Annual Report, B. G. Thomas, ed., University of Illinois, Urbana, Illinois, June 12, 2007.
[8] D. Griffin and R. Nunnington, Calcia / Alumina Diffusion Project - SEN Samples after Use, 2007, LWB Refractories, York, PA, April 17, 2007.